Supporting Information

Sulfur Encapsulation by MOF-Derived CoS$_2$ Embedded in Carbon Hosts for High-Performance Li–S Batteries

Na Zhang,[†, #] Yao Yang,[†, #] Xinran Feng,[†, §] Seung-Ho Yu,[†, ⊥]Jeesoo Seok,[†]

David A. Muller,[‡, ∆] and Héctor D. Abruña[†, *]

[†] Baker Laboratory, Department of Chemistry and Chemical Biology, Cornell University, Ithaca, New York, 14853, United States

[‡] School of Applied and Engineering Physics, Cornell University, Ithaca, New York 14853, United States

[§] Cornell High Energy Synchrotron Source (CHESS), Cornell University, Ithaca, New York 14850, United States

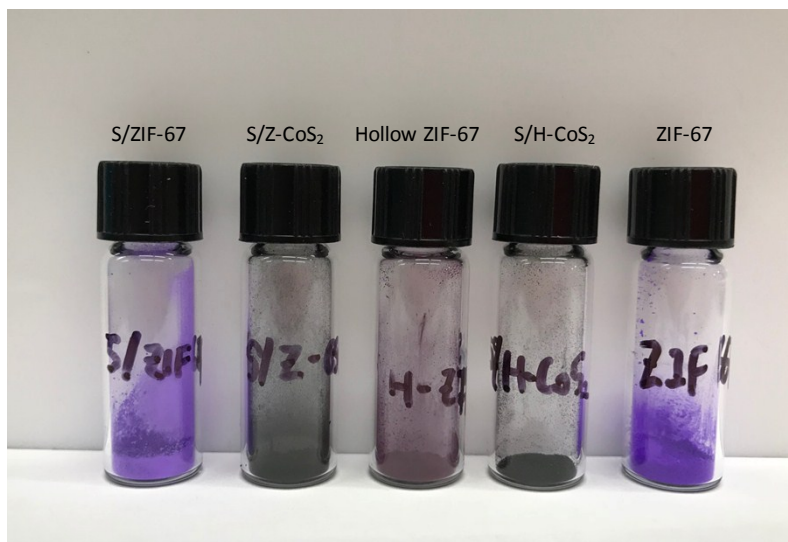[∆] Kavli Institute for Nanoscale Science, Cornell University, Ithaca, New York 14853, United States

[⊥]Department of Chemical and Biological Engineering, Korea University, 145 Anam-ro, Seongbuk-gu, Seoul 02841, Republic of Korea

* Corresponding author: hda1@cornell.edu

[#] N.Z. and Y.Y. contributed equally to this work.

This file includes:

Figure S1-S15, Table S1 and references.

Figure S1. Photographs of samples S/ZIF-67, S/Z-CoS$_2$, hollow ZIF-67, S/H-CoS$_2$ and ZIF-67. Purple S/ZIF-67 was tranformed to the black S/Z-CoS$_2$ composite via the heat treatment. After the solid ZIF-67 was treated with tannic acid, the dark purple hollow ZIF-67 was obtained. The sample turned black when the hollow ZIF-67 was mixed with sulfur and went through the heat treatment.
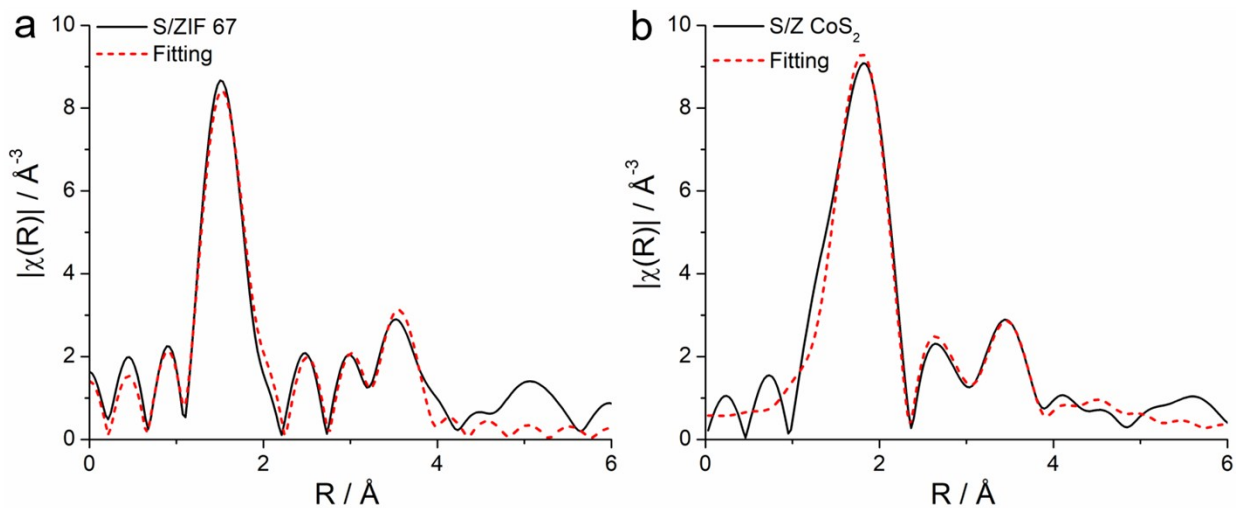
Figure S2. EXAFS profiles and fitting results for (a) S/ZIF-67 and (b) S/Z-CoS$_2$ composites. The fitting was performed within a Welch window between 1 and 5.5 Å. ZIF-67 and CoS$_2$ standard references were used to fit the experimental data. The R-factors of fittings results are 0.027 for S/ZIF-67 and 0.013 for S/Z-CoS$_2$. An R factor less than 0.05 usually indicates a good quality of fit.
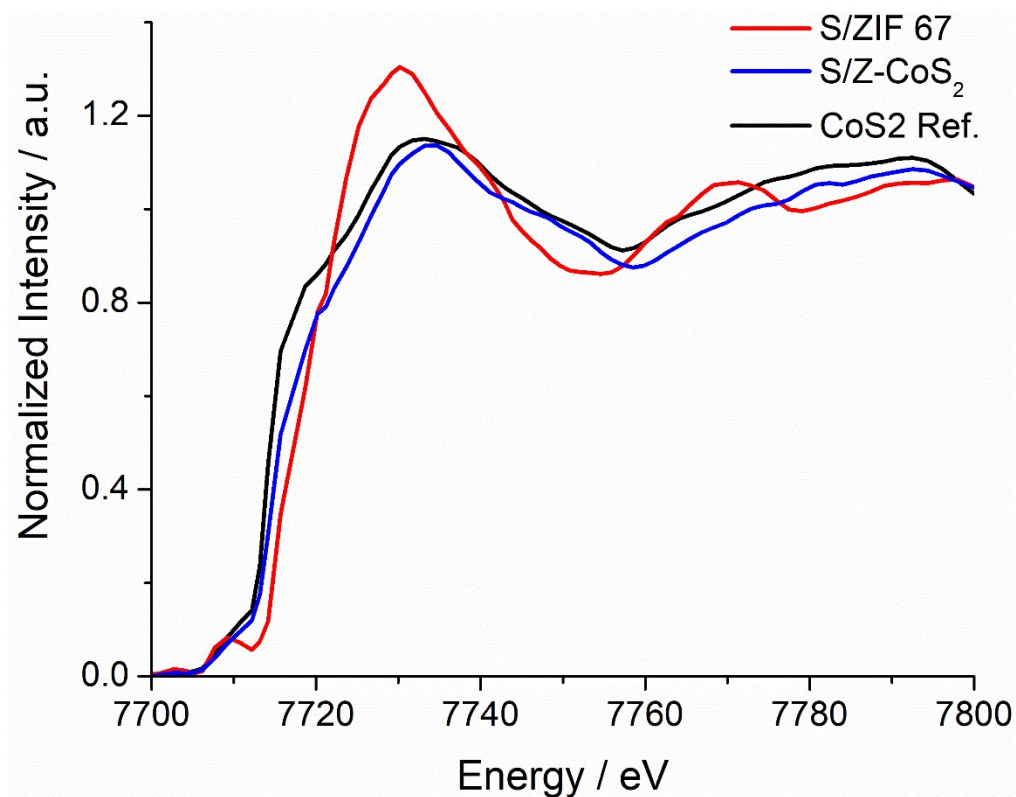
Figure S3. XANES spectra of the Co K-edge of S/ZIF-67 and S/ZIF-67 derived CoS_2 (S/Z-CoS_2) composites. The XANES spectrum of S/Z-CoS_2 exhibits similar features as for S/ZIF-67. The shift to lower energies of S/Z-CoS_2, relative to that of S/ZIF-67, suggests a decrease in the oxidation state of Co during the heat treatment.
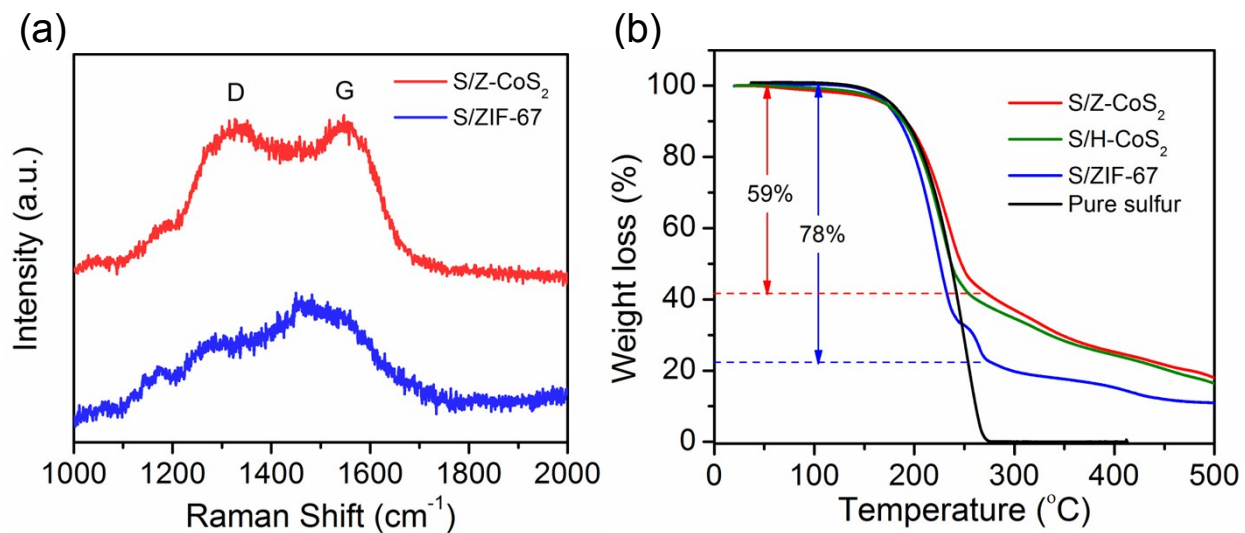
Figure S4. (a) Raman spectra of S/Z-CoS$_2$ and S/ZIF-67. (b)TGA curves of S/Z-CoS$_2$, S/ZIF-67, S/H-CoS$_2$ and pure sulfur at a ramp rate of 10 ºC min^{-1} in Ar.
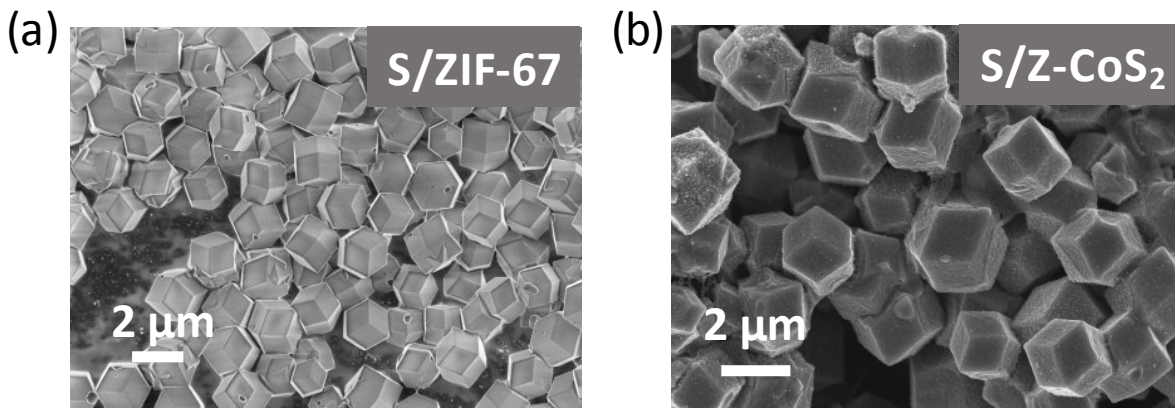

Figure S5. Low magnification SEM images of (a) S/ZIF-67 and (b) S/Z-CoS$_2$.
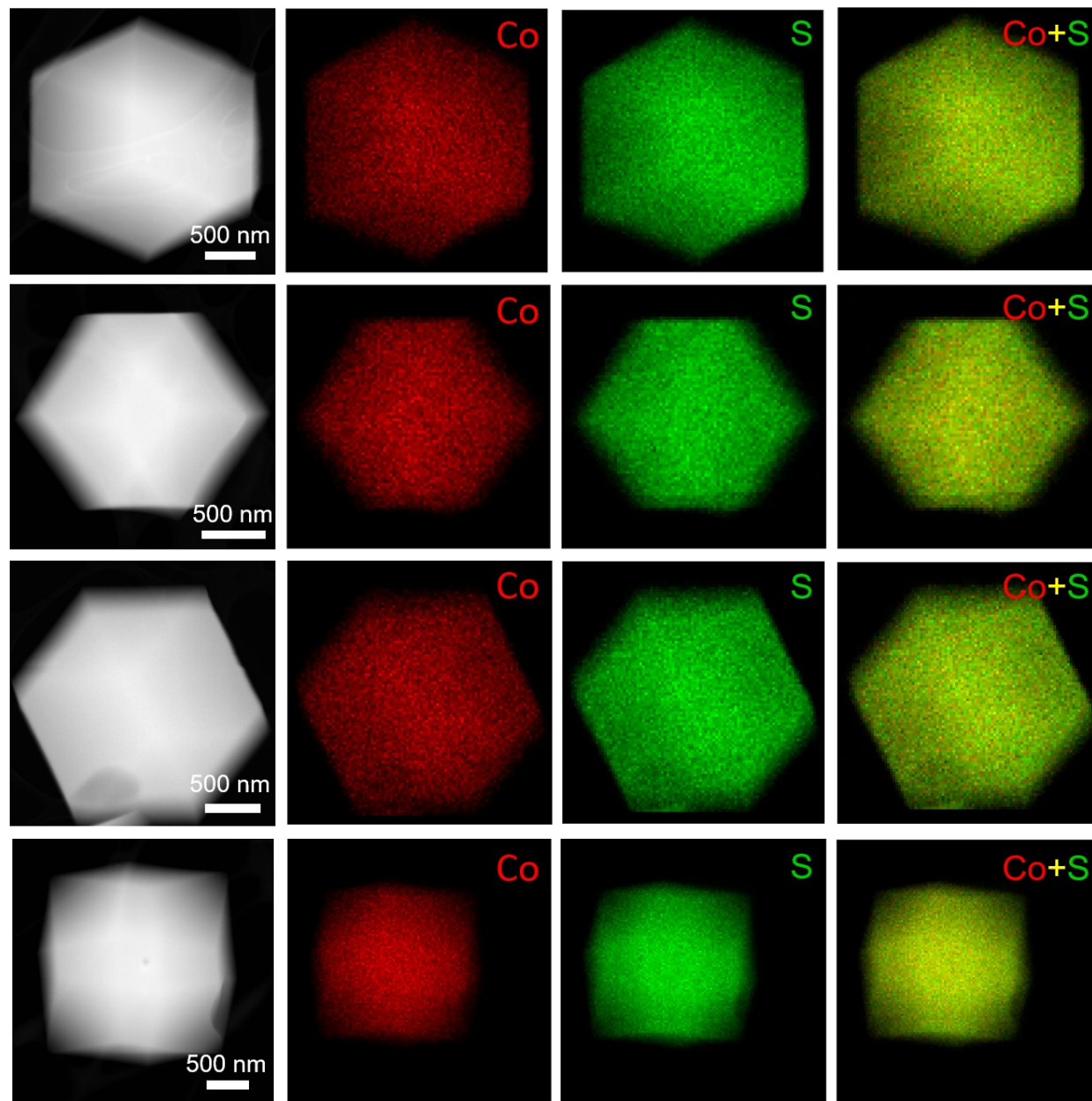
Figure S6. Cryo-STEM images of S/ZIF-67 composite particles and the corresponding maps of Co (red), S (green) and color overlay (yellow) of Co and S.

STEM image (initial) STEM image after EDX mapping
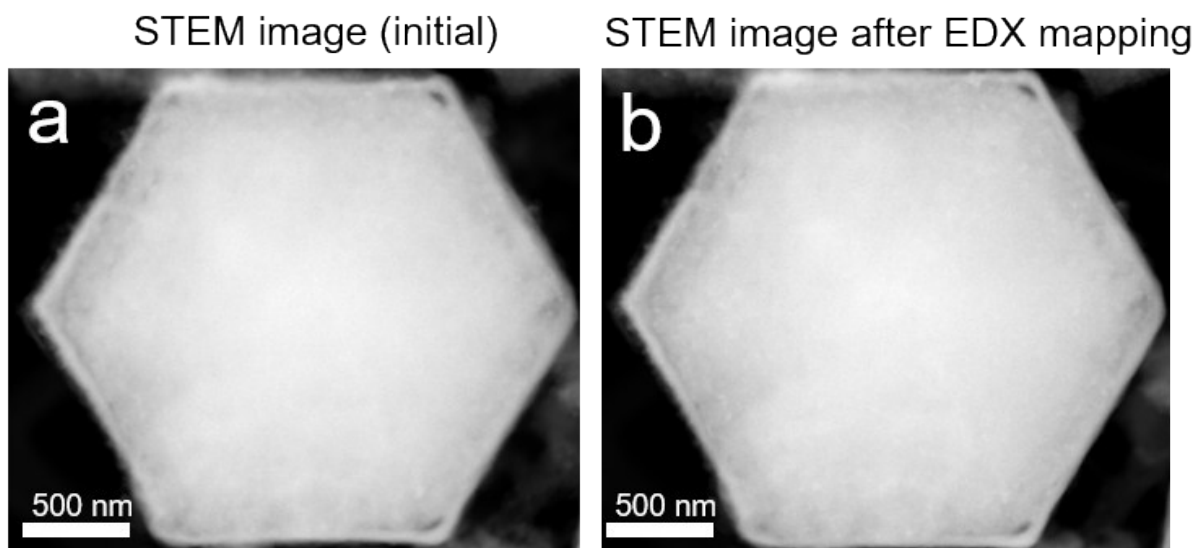
Figure S7. (a-b) Cryo-STEM images of S/ZIF-67-derived CoS$_2$ at its initial state and after EDX mapping, respectively, suggesting no noticeable beam damage during EDX mapping. EDX maps were acquired for 10 min to achieve more than 100 counts/pixel for sulfur and more than 50 counts/pixel for cobalt, with a beam voltage of 200 keV, a beam dose of 6-7 e/(nm^2 · s) and a pixel size of 128 × 128. Beam damage of all other STEM-EDX maps was routinely examined before and after EDX mapping.
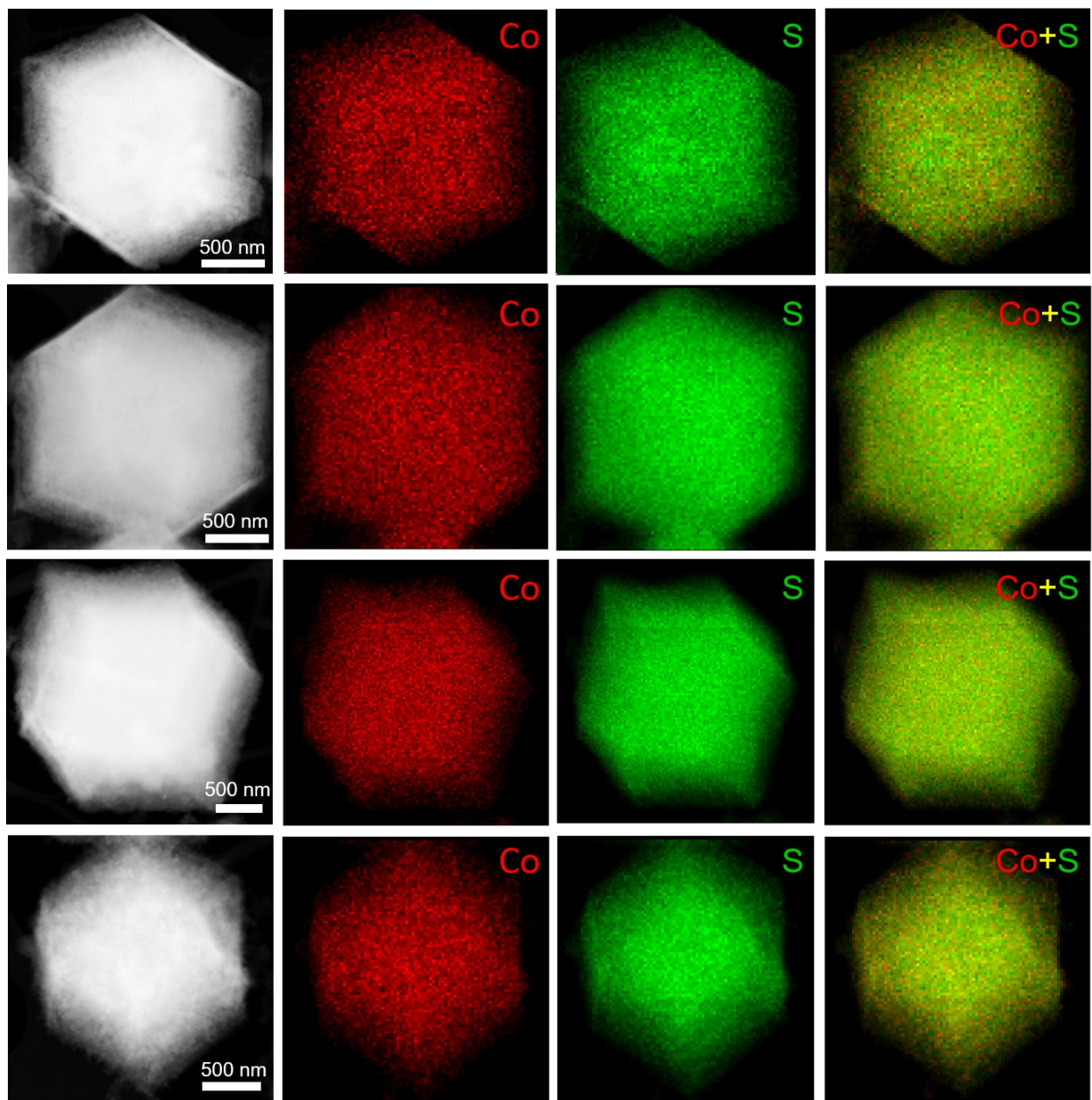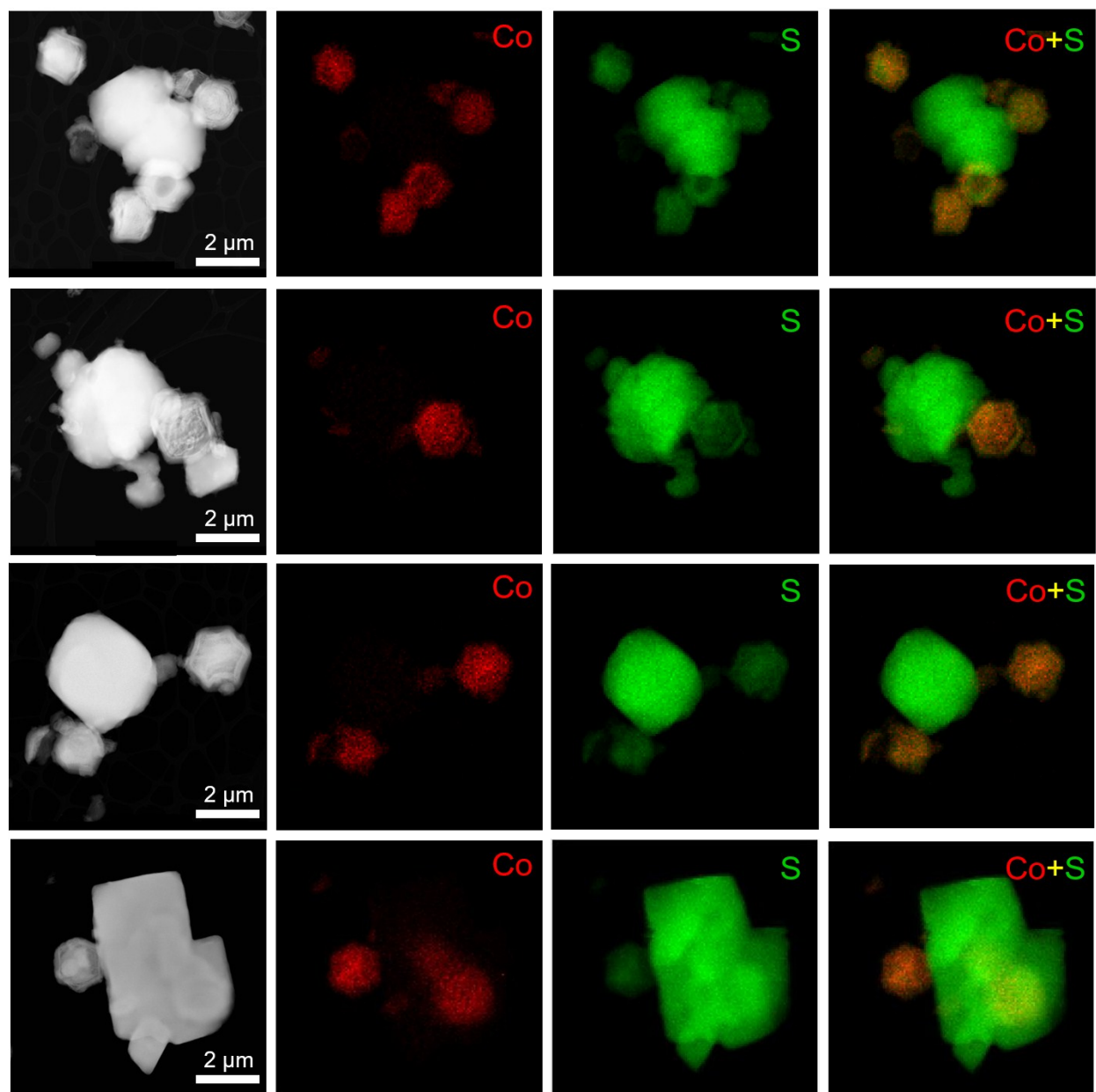
Figure S8. Cryo-STEM images of S/ZIF-67-derived CoS_2 (S/Z-CoS_2) composite particles and the corresponding EDX elemental maps of Co (red), S (green) and color overlay (yellow) of Co and S.
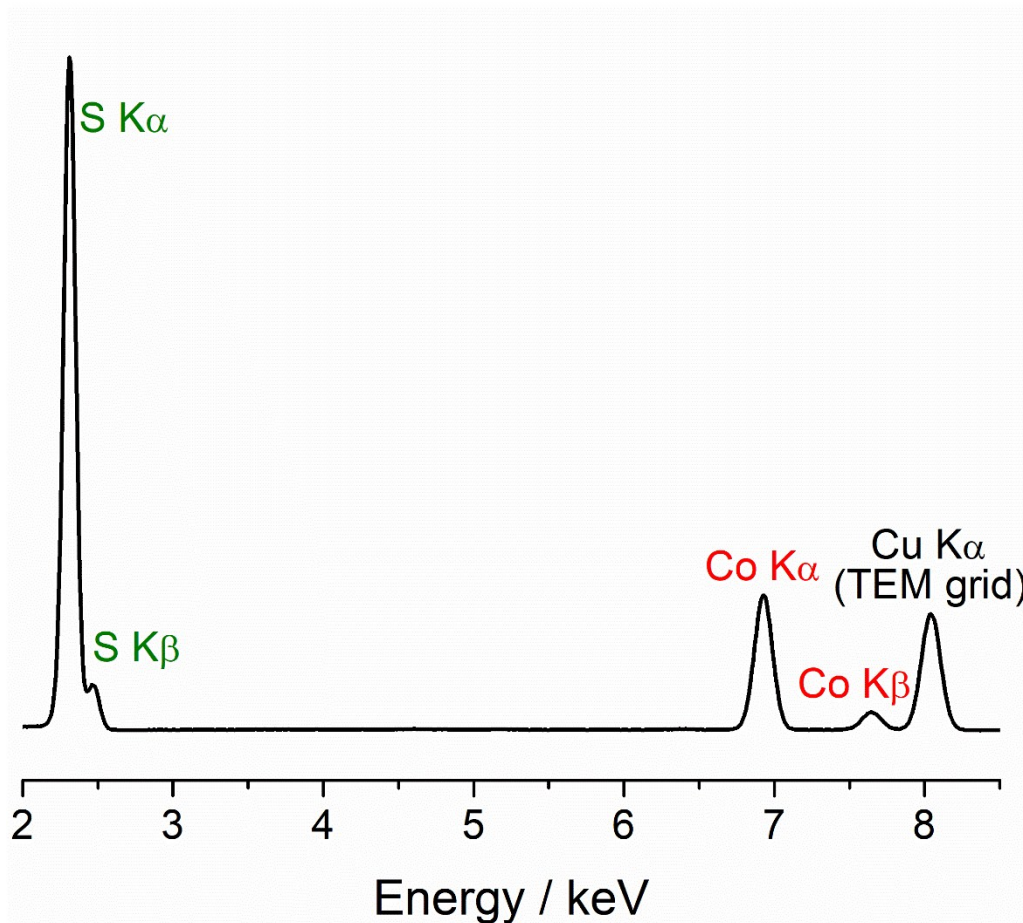
Figure S9. EDX spectrum of S/ZIF-67-derived CoS_2 composite, corresponding to the particle in Figure 3g. The S/Co atomic ratio was quantified to be 6.7:1 based on S and Co K-edges, which is quite consistent with the S/Co ratio (about 8:1) calculated from TGA results. This suggests that the majority of the sulfur is confined within the cage of ZIF-67-derived CoS_2 rather than remaining external to the particles.
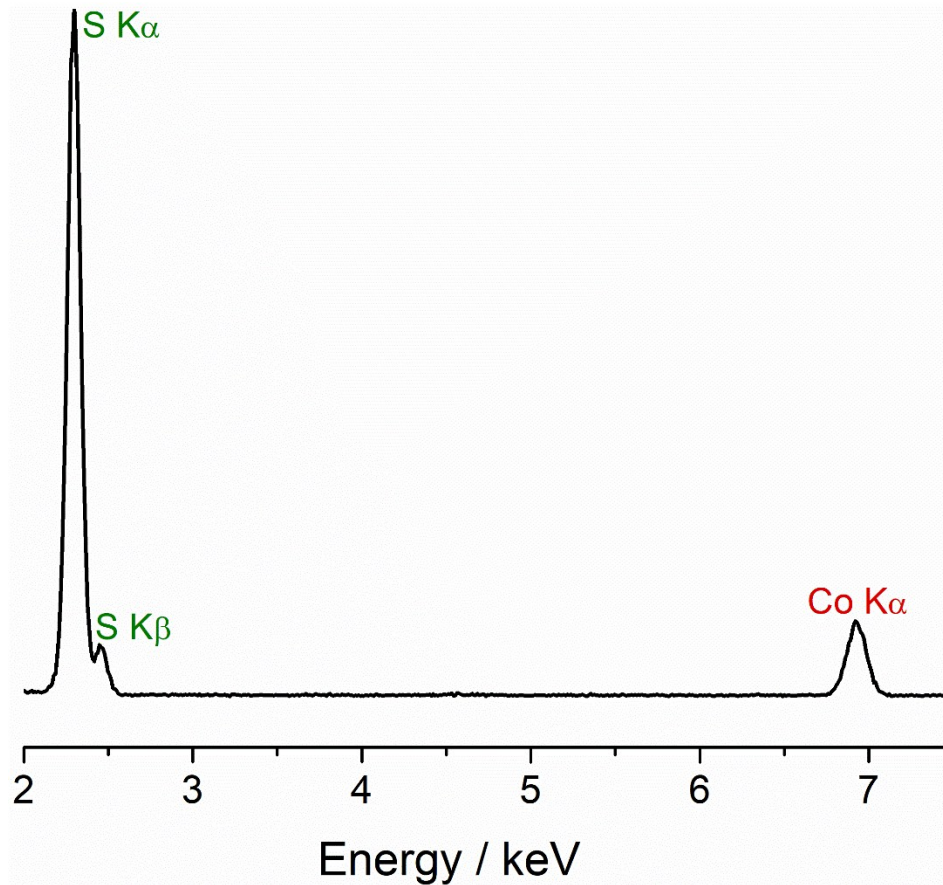
Figure S10. EDX spectrum of hollow ZIF-derived CoS_2 (H-CoS_2) composite, corresponding to the particle in Figure 4f. The S/Co atomic ratio was quantified to be around 9.5:1 based on S and Co K-edges, which is significantly larger than the S/Co ratio (2:1) in CoS_2, suggesting the existence of elemental sulfur in the cage of H-CoS_2.

Figure S11. Cryo-STEM images of S/hollow ZIF-derived CoS_2 (S/H-CoS_2) composite particles and the corresponding EDX elementa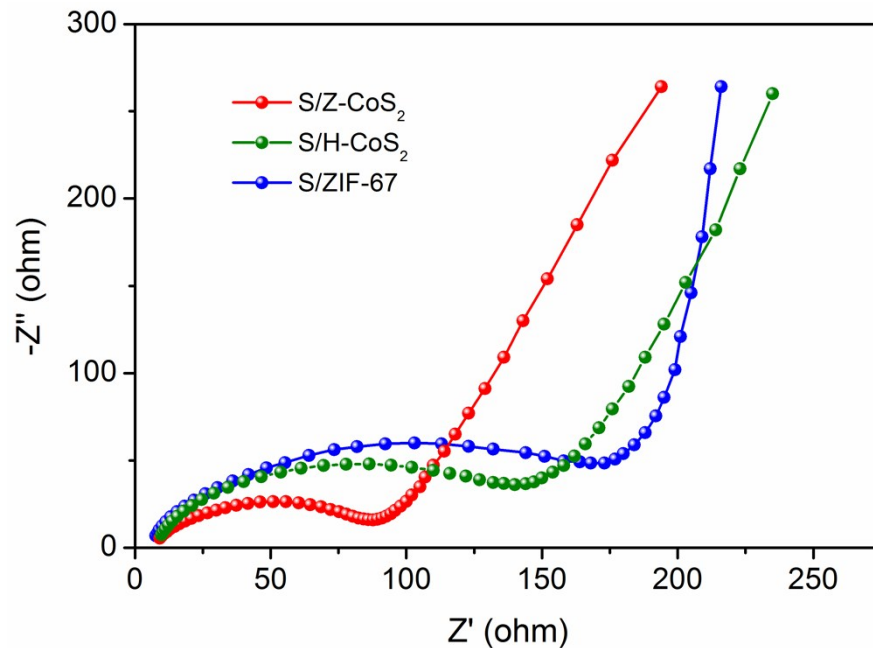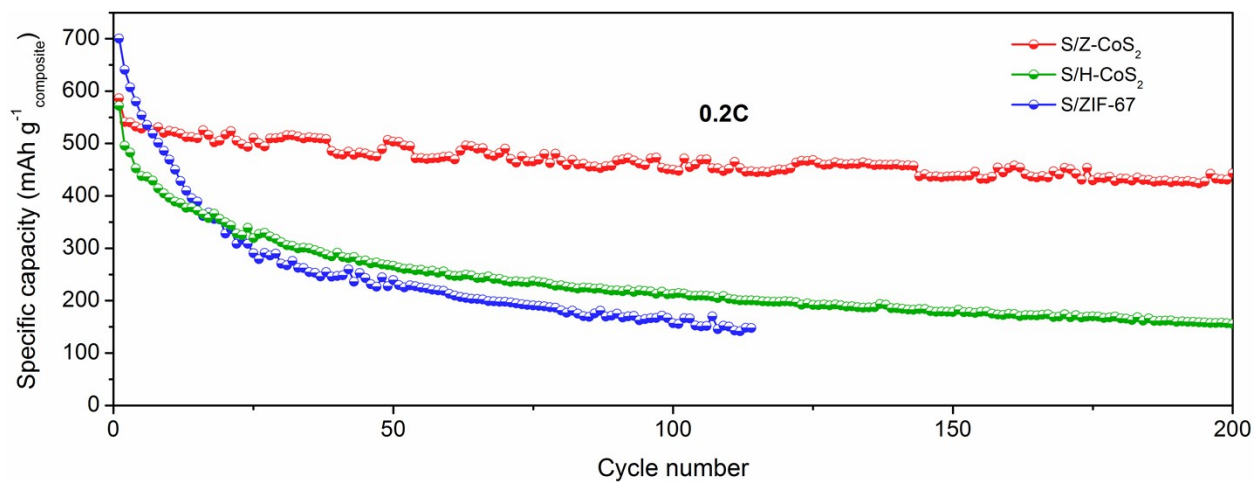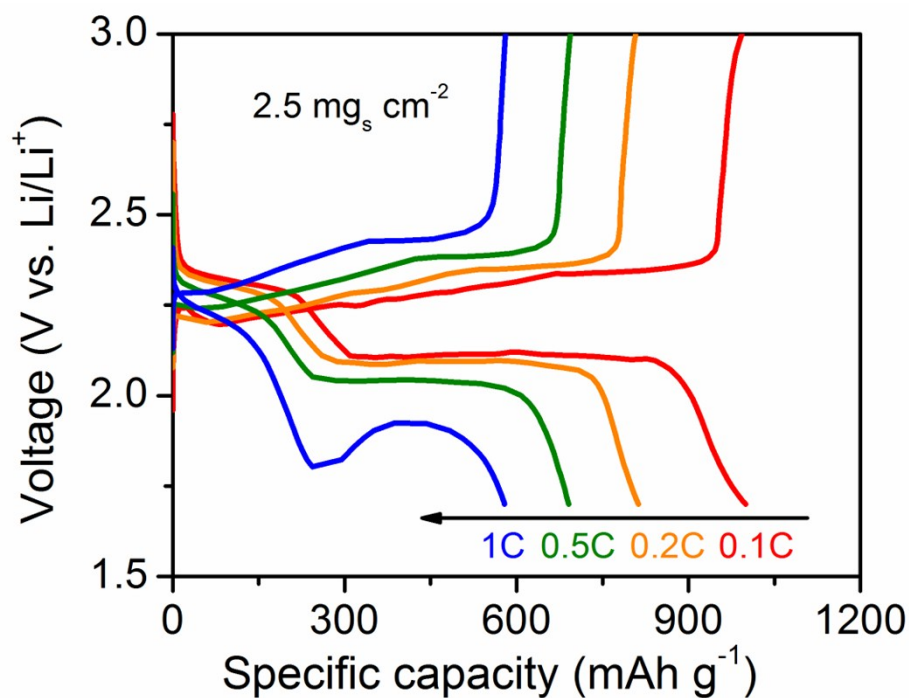l maps of Co (red), S (green) and color overlay of Co and S. Yellow suggests an overlay of Co and S elements while green indicates pure elemental sulfur.

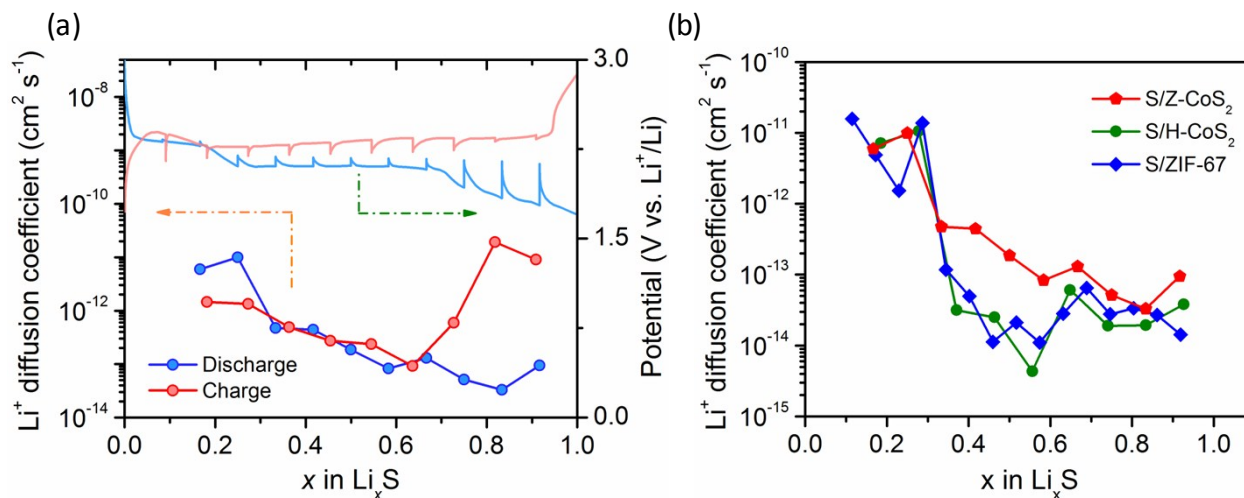**Figure S12.** EIS spectra of S/Z-CoS$_2$, S/H-CoS$_2$, and S/ZIF-67.

Figure S13. Cycling performance of S/Z-CoS$_2$, S/H-CoS$_2$, and S/ZIF-67 at 0.2 C for 200 cycles. (The capacity values were calculated based on the mass of the composite).

Figure S14. Charge/discharge profiles of S/Z-CoS$_2$ at high loading at various C-rates.

Figure S15. (a) GITT profiles of S/Z-CoS$_2$ and calculated lithium ion diffusion coefficients. (b) Comparison of lithium ion diffusion coefficients of S/Z-CoS$_2$, S/H-CoS$_2$, and S/ZIF-67.
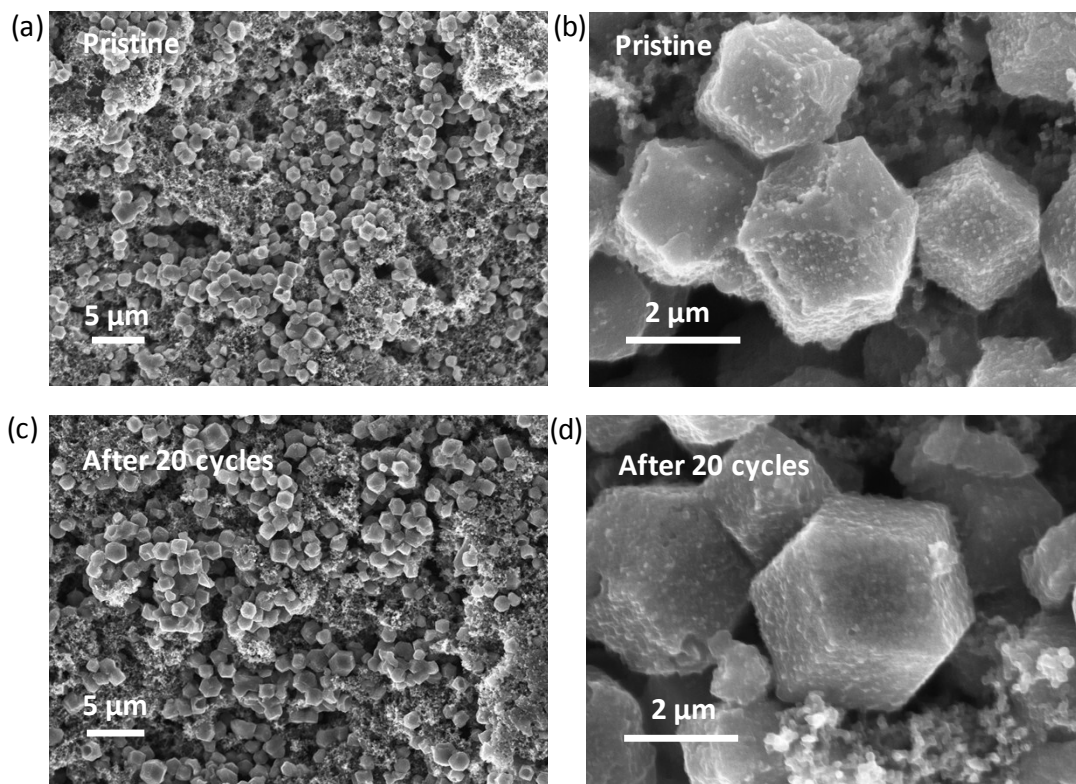
Figure S16. SEM images of S/Z-CoS$_2$ electrodes (a,b) before cycling, and (c,d) after 20 cycles.

Table S1. Comparison of electrochemical properties of S/Z-CoS$_2$ to other reported carbon, metal oxides/sulfides, MOF as sulfur hosts.

Materials	Rate performance	Cycling stability	Reference
S/Z-CoS$_2$	5C, 430 mAh g^{-1}	0.2C, 750 mAh g^{-1}, 200 cycles 1C, 440 mAh g^{-1}, 1000 cycles	This work
Hierarchical micro/mesoporous carbonaceous nanotube	2C, 616 mAh g^{-1}	1C, 558 mAh g^{-1}, 160 cycles	Ref. 1
MoO$_2$	2C, 635 mAh g^{-1}	0.1C, 570 mAh g^{-1}, 250 cycles	Ref. 2
Ni-MOF	2C, 287 mAh g^{-1}	0.2C, 520 mAh g^{-1}, 200 cycles	Ref. 3
CoS$_x$	2C, 525 mAh g^{-1}	0.1C, 423 mAh g^{-1}, 100 cycles	Ref. 4
CoS$_2$/graphene	2C, 1000 mAh g^{-1}	2C, 320 mAh g^{-1}, 2000 cycles	Ref. 5
CoS$_2$@G/CNT	4C, 480 mAh g^{-1}	0.5C, 581 mAh g^{-1}, 300 cycles	Ref. 6
Co$_9$S$_8$	2C, 880 mAh g^{-1}	0.5C, 250 mAh g^{-1}, 1500 cycles	Ref.7
Activated carbon nanofiber/Co$_3$S$_4$	2C, 752 mAh g^{-1}	1C, 610 mAh g^{-1}, 450 cycles	Ref. 8

References
1. K. Mi, Y. Jiang, J. Feng, Y. Qian and S. Xiong, *Adv. Funct. Mater.*, 2016, **26**, 1571-1579.
2. Q. Qu, T. Gao, H. Zheng, Y. Wang, X. Li, X. Li, J. Chen, Y. Han, J. Shao and H. Zheng, *Adv. Mater. Interfaces*, 2015, **2**, 1500048.
3. J. Zheng, J. Tian, D. Wu, M. Gu, W. Xu, C. Wang, F. Gao, M. H. Engelhard, J. G. Zhang, J. Liu and J. Xiao, *Nano Lett.*, 2014, **14**, 2345–2352.
4. M. Lao, G. Zhao, X. Li, Y. Chen, S. X. Dou and W. Sun, *ACS Appl. Energy Mater.*, 2017, **1**, 167–172.
5. Z. Yuan, H. J. Peng, T. Z. Hou, J. Q. Huang, C. M. Chen, D. W. Wang, X. B. Cheng, F. Wei and Q. Zhang, *Nano Lett.*, 2016, **16**, 519–527.
6. G. Zhou, H. Tian, Y. Jin, X. Tao, B. Liu, R. Zhang, Z. W. Seh, D. Zhuo, Y. Liu, J. Sun, J. Zhao, C. Zu, D. S. Wu, Q. Zhang and Y. Cui, *Proc. Natl. Acad. Sci. USA*, 2017, **114**, 840–845.
7. Q. Pang, D. Kundu and L. F. Nazar, *Mater. Horiz.*, 2016, **3**, 130–136.
8. H. Xu and A. Manthiram, *Nano Energy*, 2017, **33**, 124–129.